



Cite this: *Phys. Chem. Chem. Phys.*,
2019, 21, 22031

Unveiling the efficiency of microwave-assisted hydrothermal treatment for the preparation of SrTiO₃ mesocrystals†

Luis F. da Silva,^a Ariadne C. Catto,^a Waldir Avansi Jr.,^a Alexandre Mesquita,^b Lauro J. Q. Maia,^c Osmando F. Lopes,^d Máximo Siu Li,^e Mário L. Moreira,^f Elson Longo,^g Juan Andrés^h and Valmor R. Mastelaro^e

Material processing has become essential for the proper control, tuning and consequent application of the properties of micro/nanoparticles. In this case, we report herein the capability of the microwave-assisted hydrothermal (MAH) method to prepare the SrTiO₃ compound, as a case study of inorganic compounds. Analyses conducted by X-ray diffraction, X-ray photoelectron and X-ray absorption spectroscopies confirmed that the MAH route enables the formation of pristine SrTiO₃. The results indicated that the combination of thermal and non-thermal effects during the MAH treatment provides ideal conditions for an efficient and rapid synthesis of pristine SrTiO₃ mesocrystals. Scanning electron microscopy images revealed a cube-like morphology (of ca. 1 μm) formed via a self-assembly process, influenced by the MAH time. Additionally, photoluminescence measurements revealed a broad blue emission related to intrinsic defects, which decreased with the MAH synthesis time.

Received 21st May 2019,
Accepted 16th September 2019

DOI: 10.1039/c9cp02893e

rs.c.li/pccp

1. Introduction

The processing of ceramic materials with multifunctional properties has been attracting the attention of researchers^{1–9} aiming to prepare micro/nanostructured inorganic semiconductors through the exploration of a variety of physical and chemical approaches.^{2,10–17} Despite their capability in obtaining such semiconductors, most of the approaches spend a large amount of energy and require long synthesis times.^{2,13,14,18–20} In this context, the microwave-assisted

hydrothermal (MAH) route has been considered a clean, versatile, fast, and highly efficient method to obtain organic and inorganic compounds.^{7,21–23} Microwave energy has the potential to be ubiquitous and greatly contribute to the synthesis of materials in almost all areas of synthetic chemistry fields,^{2,7,13,14,18,19,24,25} considering that it requires short times and relatively low temperatures (usually <200 °C) in comparison with conventional heating methods.^{14,26} This route also contributes to suppressing side reactions, improving the degree of reproducibility.^{10,13,14}

In 1990, Komarneni and co-workers investigated the preparation of oxide materials via microwave-assisted treatment.² They reported that this methodology improved the crystallization kinetics of various inorganic compounds.² In the past few years, there has been increasing interest in improving the MAH route for the synthesis of micro/nanocrystals, since it provides not only a simple and fast way to obtain these materials, but also because its homogeneous heating minimizes thermal gradient effects with the formation of oriented structures with unique or enhanced properties.^{13,14,18,19,27}

De La Hoz and co-workers described that the importance of microwave irradiation during chemical synthesis could be related to thermal and non-thermal effects.¹⁹ According to the authors, the thermal effects are the solution superheating and the presence of hot-spots, while the non-thermal effects are the highly polarized electric field and those related to mobility and diffusion that increase the probabilities of effective contacts.¹⁹

^a Laboratory of Nanostructured Multifunctional Materials, Federal University of São Carlos, Rodovia Washington Luiz, km 235, 13565-905, São Carlos, SP, Brazil.

E-mail: lfsilva83@gmail.com; Tel: 55 16 35091524

^b Institute of Geosciences and Exact Sciences, São Paulo State University, Unesp, 13506-900, Rio Claro, SP, Brazil

^c Institute of Physics, Federal University of Goiás, Alameda Palmeiras s/n, 74690-900, Goiânia, GO, Brazil

^d Institute of Chemistry, Federal University of Uberlândia, 38400-902, Uberlândia, MG, Brazil

^e Institute of Physics of São Carlos, University of São Paulo, Avenida Trabalhador São Carlos, 13566-590, São Carlos, SP, Brazil

^f INCTMN, Physical and Mathematics Institute (IFM), Universidade Federal de Pelotas, Campus Universitário Capão do Leão, 96010-900, Pelotas, RS, Brazil

^g Center for Development of Functional Materials, Federal University of São Carlos, Rodovia Washington Luiz, km 235, 13565-905, São Carlos, SP, Brazil

^h Departamento Química-Física y Analítica, Universitat Jaume I, Castelló E-12080, Spain

† Electronic supplementary information (ESI) available: XRD patterns and FTIR spectra of samples SAM2, SAM3 and SAM4. See DOI: 10.1039/c9cp02893e

Motivated by such versatility and efficiency, the MAH method has been used to obtain different micro/nanocrystalline compounds.^{13,14,19,28–30} Strontium titanate (SrTiO₃) has attracted attention because of its remarkable multifunctional properties.^{3,31–37} Moniruddin and co-workers demonstrated the potential of pristine SrTiO₃ nanoparticles as catalysts for the production of H₂ gas *via* a water-splitting process.³⁵ In the past decade, our research group studied the pristine and doped nanostructured SrTiO₃ applied as photocatalysts and a gas-sensing layer. To do so, different methodologies were used, such as electron beam vapor deposition, the polymeric precursor method, conventional hydrothermal routes and the MAH method.^{24,38–43} Regarding the MAH route, it was successfully used to prepare SrTiO₃ powders, allowing proper control over the crystal shape, photoluminescence properties and assembly process of the nanoparticles by an appropriate choice of titanium precursor as well as synthesis time.^{23,24,27,39}

In one of these previous studies, we demonstrated the relationship between structural properties and photocatalytic activity of SrTiO₃ obtained *via* the MAH route, where we could observe a high disorder degree in the local structure around Ti atoms beyond the presence of some fivefold coordinated Ti atoms, leading to a photocatalytic improvement of the as-obtained samples of pristine SrTiO₃.²⁴ Following this line of research, the aim of this work is threefold: (i) to demonstrate the efficiency and potentiality of the MAH method in obtaining pristine SrTiO₃ crystals; (ii) to show the potential of this route for designing functional materials with superior properties and; (iii) to present and investigate the relationship between microwave-assisted hydrothermal treatment and photoluminescent properties. To achieve these purposes, different techniques such as X-ray diffraction (XRD), X-ray absorption near edge structure (XANES) spectroscopy, X-ray photoelectron spectroscopy (XPS), electron paramagnetic resonance (EPR), photoluminescence (PL) spectroscopy, and field emission scanning electron microscopy (FE-SEM) were employed to characterize the obtained samples.

2. Experimental section

2.1. Synthesis and characterization of SrTiO₃

To evaluate the effect of the MAH treatment on the preparation of the SrTiO₃ compound, two reaction mixtures were prepared, as reported in ref. 24. Strontium chloride (SrCl₂·6H₂O; 99.9%) and titanium oxysulfate (TiOSO₄·xH₂SO₄·yH₂O solution; 99.9%) reagents purchased from Sigma-Aldrich Corporation were used. First, TiOSO₄ and SrCl₂ (0.01 M, Sr:Ti = 1:1) were added to 50 mL of deionized water, followed by another 50 mL of 6 M KOH solution under constant stirring for 30 min. Afterwards, the reaction mixture was washed with deionized water and isopropyl alcohol, and then dried for 12 h at 80 °C. The obtained sample was labelled as SAM1.

2.1.1. MAH synthesis vs. thermal annealing. In order to demonstrate the efficiency of the MAH synthesis compared to conventional thermal annealing, the sample SAM1 was weighted and then divided into three equal portions. Two portions

were annealed in an electric oven under air atmosphere for 2 h, one at 300 °C, and the other at 750 °C, both at a heating rate of 10 °C min⁻¹. The last portion of the sample was maintained as-obtained, *i.e.*, without any treatment.

2.1.2. Longer MAH synthesis time. To study the influence of synthesis time, the precursor solution was heat-treated in the MAH system for 10 min (SAM2), 320 min (SAM3), and 640 min (SAM4). To this end, the reaction mixture was put into a 110 mL Teflon autoclave, which was in turn sealed and placed inside the custom-built microwave-assisted hydrothermal (MAH) system. The solution was then treated at 140 °C with a heating rate of 140 °C min⁻¹ under an auto-generated pressure of 3 bar. At the end of the synthesis, the precipitated powder was washed and dried following the same procedure steps mentioned above.

2.2. Characterization techniques

The samples were characterized by X-ray diffraction (XRD) at $2\theta = 20^\circ$ to 60° with a step size of 0.02° , at a scanning speed of 2° min^{-1} , using CuK α radiation (Rigaku, RotaflexRU200B). The structure was refined using the Rietveld method and the General Structure Analysis System (GSAS) package with the EXPGUI graphical user interface. The average crystallite size was calculated from the full-width at half-maximum (FWHM) of the (110) XRD peak in the Scherrer equation.³⁸ The FWHM value of the XRD peak due to instrumental broadening was considered using the Si sample as a reference. X-ray absorption near-edge structure (XANES) measurements were performed at the XAFS2 beamline at the Brazilian Synchrotron Light Laboratory (LNLS). The Ti K-edge XANES spectra were collected in transmission mode at room temperature in the range of 4910 to 5200 eV with an energy step size of 0.3 eV around the edge, following the already reported experimental conditions.^{31,36,44} For the XANES analysis, the background was removed from all the spectra, which were then normalized by first extended X-ray absorption fine structure (EXAFS) oscillation using MAX software.⁴⁵ X-ray photoelectron spectroscopy (XPS) analyses were performed on a ScientaOmicron (model ESCA+) spectrometer using monochromatic AlK α ($h\nu = 1486.6 \text{ eV}$) radiation. The binding energies were corrected for charging effects by assigning a value of 284.8 eV to the adventitious C 1s line.

Morphological properties of the samples were characterized using a field emission scanning electron microscope (FE-SEM, Zeiss Supra35) operated at 5 kV in different magnifications. Room-temperature photoluminescence (PL) spectra were collected using a Thermal Jarrel-Ash Monospec 27 monochromator and a Hamamatsu R446 photomultiplier linked with a data acquisition system consisting of an SR-530 lock. All the samples were excited by 350 nm wavelength light from a krypton ion laser (Coherent Innova) and the nominal output power of the laser was kept at 200 mW.

Electron paramagnetic resonance (EPR) measurements of pristine SrTiO₃ samples were collected using a Bruker Elexsys line model E-580 X-band spectrometer. The microwave frequency used was 9.5 GHz with a power of 8.025 mW. Measurements were taken at a temperature of 10 K with a magnetic field ranging from 500 to 4500 G.

3. Results and discussion

3.1. The efficiency of the MAH approach

XRD patterns of the samples SAM1 (before MAH treatment) and SAM2 (after MAH treatment) are shown in Fig. 1. The XRD pattern of SAM1 can be indexed to various crystalline phases identified as: SrTiO₃ (JCPDS file 35-0734), SrSO₄ (JCPDS file 05-0593), SrCl₂·6H₂O (JCPDS file 06-0073), SrCO₃ (JCPDS file 05-0418) and K₂Ti₆O₁₃ phase (JCPDS file 74-0275). In contrast, the XRD pattern of SAM2 reveals that when submitted to MAH treatment, it exhibits only reflections assigned to cubic perovskite SrTiO₃ phase.^{23,24,27}

Before MAH treatment, the reactants were mixed under alkaline conditions at room temperature to form the aforementioned crystalline phases, SrSO₄ being the major phase found. This may be associated with the low solubility of SrSO₄ under alkaline ($K_{sp} = 3.8 \times 10^{-7}$) conditions.⁴⁶ Nevertheless, when the reaction mixture undergoes MAH treatment, the pristine SrTiO₃ phase can be obtained, as seen in Fig. 1. Some researchers described that the hydrothermal route, especially the microwave-assisted one, enhances the solubility and mobility of the ionic species as a result of water viscosity and polarization reductions related to the electric field component of the electromagnetic wave.^{14,46} Therefore, such a treatment is capable of solubilizing SrSO₄, thus providing Sr(II) ions to react with Ti species, consequently forming pristine SrTiO₃.

To confirm the efficiency of the MAH method to obtain the SrTiO₃ pristine compound, the as-obtained sample SAM1 was annealed in an electric oven for 2 h at 300 °C, and 750 °C. The XRD patterns of the samples after thermal annealing are shown in Fig. 2. All the samples presented a mixture of crystalline phases. It is interesting to note that independent of the annealing temperature (in the range here investigated), the conventional heating was ineffective in providing the necessary conditions to obtain the pristine SrTiO₃. Therefore, the presented results confirm the efficiency of the MAH method in synthesizing a pure SrTiO₃ compound in a shorter time and at a lower temperature.

3.2. The influence of longer MAH synthesis time

To obtain further details on the processing of the SrTiO₃ compound using the MAH method, we studied the influence

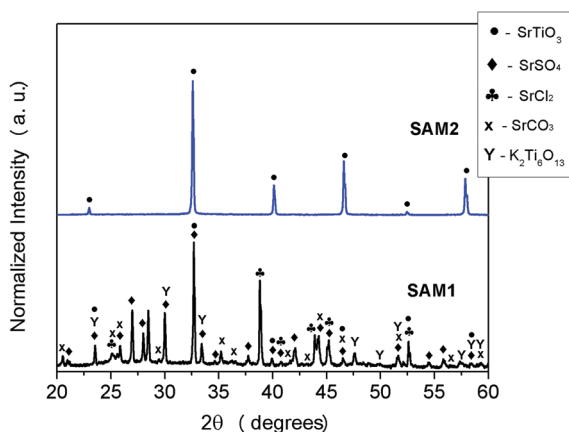


Fig. 1 XRD patterns of samples SAM1 and SAM2.

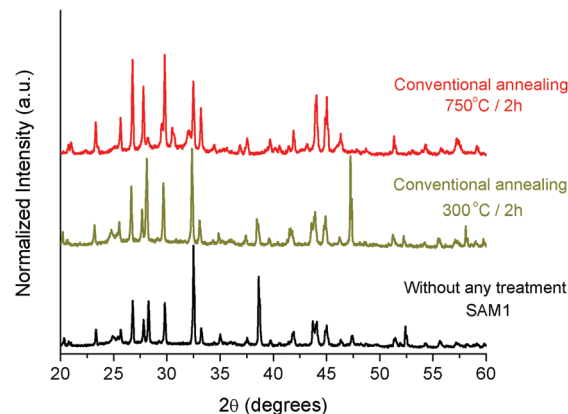


Fig. 2 XRD patterns of the sample SAM1 as-obtained (without any treatment), and then annealed in an electric oven for 2 hours at 300 °C, and 750 °C.

of longer MAH synthesis time on the local structure around the Ti atoms, on the surface electronic structure, and on the PL emission of the compound. For this purpose, the reaction mixtures were treated in the MAH system at 140 °C for 10 min (SAM2), 320 min (SAM3) and 640 min (SAM4), where the synthesis parameters, such as pressure, heating rate and precursors and their concentrations, were kept constant. Fig. S1 and S2 (ESI[†]) shows the XRD patterns of samples SAM2, SAM3 and SAM4, all reflections being indexed to the cubic perovskite structure of the SrTiO₃ phase (JCPDS file 35-0734) without any spurious phase.

The influence of MAH time on the crystallite size and the lattice parameter are presented in Table 1. A reduction of both structural parameters with MAH treatment time can be observed. The behavior can be attributed to the larger amount of energy provided during the MAH treatment, which corroborates to reduce the defects in the SrTiO₃ network. Note that the literature reports an a_0 value of approximately 3.905 Å.^{23,37}

Fig. 3 shows the Ti K-edge XANES spectra of the samples SAM1, SAM2, SAM3 and SAM4 and the spectrum of the crystalline SrTiO₃ (used as a reference compound) prepared *via* the polymeric precursor method, here designated as c-SrTiO₃.^{38,42} The spectra revealed four pre-edge transitions, labeled as P1, P2, P3 and P4, as seen in the inset of Fig. 3. The physical origin of these electronic transitions is described elsewhere.^{24,36,42}

First, it can be seen that the spectra of the samples synthesized *via* the MAH route (SAM2, SAM3 and SAM4) are quite similar to the c-SrTiO₃ spectrum, which in turn is different from the SAM1 spectrum. Such results confirm that samples obtained

Table 1 Average XRD crystallite size and lattice parameter (a_0) estimated from XRD patterns of the samples treated at 140 °C

Sample	MAH time (min)	Average crystallite size (nm)	a_0 (Å)	χ^2	R_{wp} (%)
SAM2	10	74(1)	3.9203(1)	4.52	11.96
SAM3	320	49(1)	3.9181(1)	4.52	7.04
SAM4	640	45(1)	3.9182(1)	5.91	7.85

χ^2 : is the square of goodness-of-fit indicator; R_{wp} : considered profile.

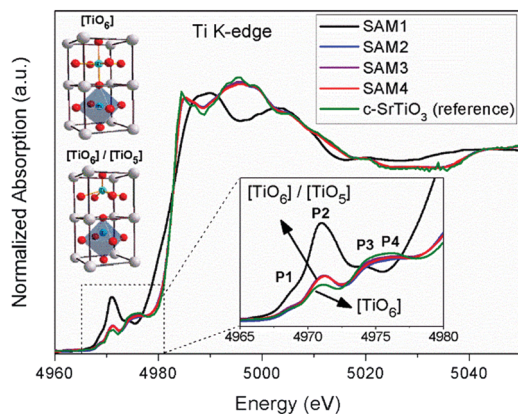


Fig. 3 Ti-K edge XANES spectra of samples SAM1, SAM2, SAM3 and SAM4 and the c-SrTiO₃ reference. The inset shows the pre-edge XANES region, illustrating the presence of TiO₅ and TiO₆ clusters.

via the MAH route have a structure similar to the c-SrTiO₃ reference at short- and medium-range order around Ti atoms.

Regarding the influence of MAH synthesis time, the analysis of the pre-edge region shows that the intensity of peak P2 is higher for samples obtained *via* the MAH method (SAM2, SAM3 and SAM4) than for c-SrTiO₃. Our research group has extensively investigated the local structure of ATiO₃ (A = Sr, Ba, Pb, or Ca) compounds using XAS spectroscopy.^{8,23,24,27,31,36,42} These investigations reveal that the intensity of the peak P2 is directly related to the local symmetry of Ti cations.^{24,31,42,47} Indeed, such an electronic transition is related to e_g orbitals, linked to Ti–O bonding, being sensitive to symmetry variations in the Ti environment.^{23,24,48–51} Thus, the pre-edge region spectrum of c-SrTiO₃ (inset of Fig. 3) is typical of titanates, where it is possible to find Ti cations coordinated by six oxygen anions, *i.e.*, formed by TiO₆ clusters.^{23,24,31} In contrast, it can be noticed that the peak P2 is more intense in SAM2, SAM3 and SAM4 than in c-SrTiO₃, suggesting the existence of a mixture of TiO₅/TiO₆ clusters in samples obtained *via* the MAH route, as illustrated in Fig. 3.

It is important to note that although XRD results have confirmed a perfect long-range order for SrTiO₃ samples prepared *via* the MAH route, the XANES spectra indicate a local disorder structure in the environment around Ti cations, which is not affected by the synthesis time. The MAH system allows high reaction rates that favored here a fast crystallization of the SrTiO₃ phase. Despite exhibiting high order at long-range, this structure also presents a disorder in the local environment around Ti atoms.

The morphology of the as-obtained samples was studied *via* FE-SEM images. Fig. 4(a and b) show that SAM1 (without MAH treatment) consists of a non-homogeneous agglomeration of particles. These results are expected, since this sample contains different crystalline structures observed by XRD and XANES analyses. Fig. 4(c–f) reveal the formation of cube-like superstructures (or mesocrystals) as a consequence of the assembly of smaller cubes induced by MAH treatment.²⁴ In this way, even with a longer MAH time, such as 320 min, the as-observed

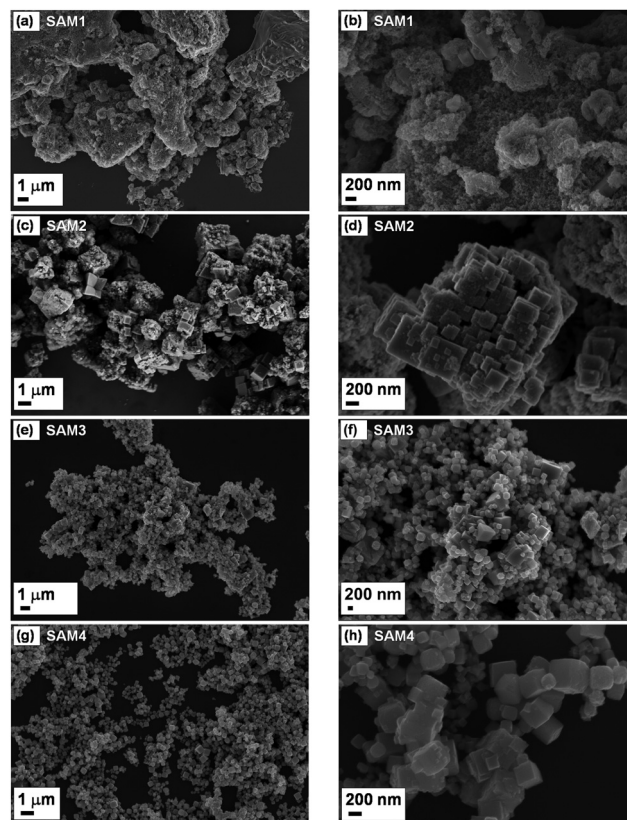


Fig. 4 FE-SEM images of samples (a and b) SAM1, (c and d) SAM2, (e and f) SAM3, and (g and h) SAM4.

morphology remains similar. Nevertheless, for samples treated during 640 min (SAM4), the cubes became more homogeneous and well-defined exhibiting less assembled smaller cubes, as evidenced in Fig. 4(g and h).

It is known that the synthesis method plays an important role in order to obtain SrTiO₃ micro/nanostructures with different morphologies.^{27,52} Our research group reported that the mediation of this process occurs due to the presence of OH groups adsorbed on the nanocrystals, leading to the formation of a specific configuration in which such crystals organize themselves into desired patterns through an oriented attachment (OA) mechanism, which could produce a defective single crystal with a spherical or cubic shape.²³ The presence of OH species on the sample surface was revealed by FTIR spectra, as displayed in Fig. S3 (ESI[†]). Thus, these small aggregated nanocrystals originated from the OA mechanism are responsible for increasing the crystal size when the coalescence occurs.^{23,24,27,39,53,54}

Fig. 5(a) shows the XPS survey spectra of the representative samples SAM2 and SAM4 and the c-SrTiO₃ reference. The peaks in these spectra were indexed, revealing the presence of the elements Sr, Ti, O and C. Beyond the peaks previously observed in the SAM4 XPS spectrum, it is also possible to identify a small peak assigned to K, a remainder of the mineralizing source.

In the high-resolution Sr 3d XPS spectra shown in Fig. 5(b), it is possible to observe two strong peaks located at 132.6 eV and 134.3 eV, which correspond to Sr(II) species on the surface

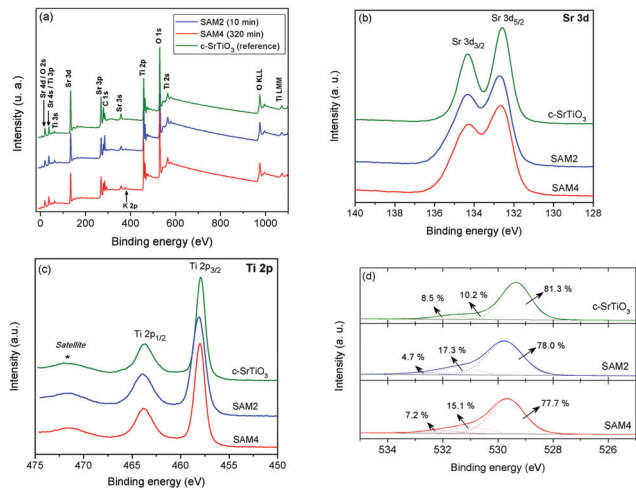


Fig. 5 XPS spectra of samples SAM2 and SAM4 and c-SrTiO₃. (a) Survey scan, (b) Sr 3d, (c) Ti 2p, and (d) O 1s core level spectra.

of the samples.^{55–57} The deconvolution of the Ti 2p XPS spectra, Fig. 5(c), reveals two main peaks at 458.3 and 464.0 eV attributed to Ti 2p_{3/2} and Ti 2p_{1/2} doublet core levels,^{55,56,58} whose binding energy values were assigned to Ti(IV) species in SrTiO₃.^{55–60} The correspondent O 1s high-resolution spectra of SAM2 and SAM4 samples and that of the c-SrTiO₃ reference compound were deconvoluted into three components, as illustrated in Fig. 5(d). The standard deviation value of the peak area was *ca.* $\pm 1.5\%$. The spectra exhibited similar characteristics, with the peak at around 529 eV corresponding to the oxygen lattice at the SrTiO₃ network.^{55,56,58,61} The second component located at approximately 531 eV was attributed to O²⁻ and O⁻ ions in the oxygen-deficient regions caused by oxygen vacancies.⁶⁰ Tan and co-workers investigated the surface properties of SrTiO₃ nanocrystals applied as photocatalysts.⁶⁰ The peak at around 532 eV was attributed to oxygen adsorbed to the sample surface.⁶⁰ As seen in Fig. 5(d), the peak area attributed to oxygen vacancies is higher in the samples obtained *via* the MAH route when compared to the reference compound (c-SrTiO₃), indicating the presence of a higher concentration of surface oxygen vacancies in these samples. Furthermore, it can be observed that the increase in the MAH time led to a decrease in this peak area, suggesting a reduction of the oxygen vacancies on the sample surface.

Fig. 6 shows the PL emission spectra of the samples SAM2, SAM3 and SAM4 and the c-SrTiO₃ reference. All the spectra exhibit a broad-band emission centered at *ca.* 470 nm (2.64 eV). The broad blue emission band is typical of compounds exhibiting intermediate electronic levels within the band gap where the relaxation process occurs along several paths, either involving additional levels located at the top of the O 2p valence band and lower conduction band 3d orbitals of Ti.^{23,31,38,62–65} Fig. 6 reveals a decrease in the PL intensity with MAH time, reaching a similar shape (intensity and profile) to the c-SrTiO₃ spectrum. As suggested by XPS results related to O vacancies, this behavior confirms that longer MAH times favor a reduction in the concentration of intrinsic defects created during the rapid crystallization process of the SrTiO₃ phase *via* the MAH method,

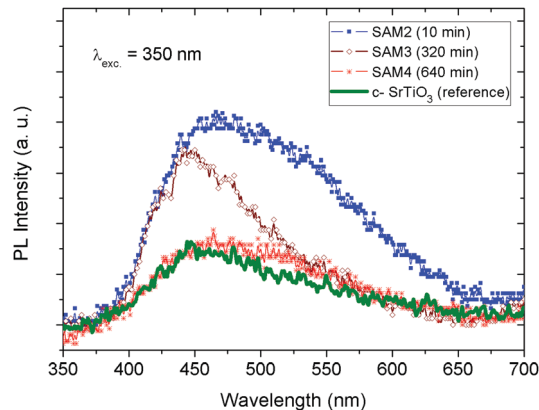


Fig. 6 PL spectra of samples SAM2, SAM3 and SAM4 at room temperature. For comparison purposes, the PL spectrum of the reference sample (c-SrTiO₃) was inserted.

which are probably oxygen vacancies. All these features show that the structural quality can be improved by increasing the reaction time, attaining the purpose of this work.

The presence of oxygen vacancies, previously mentioned, was confirmed by using the electron paramagnetic resonance (EPR) technique. The EPR signal can be assigned to the paramagnetic oxygen vacancies,^{60,66} which allows the formation of intermediary energy levels in the SrTiO₃ band gap, and consequently leads to broad PL emission presented in Fig. 6.

Fig. 7 shows the electron paramagnetic resonance (EPR) spectra of samples SAM2, SAM3 and SAM4. The spectra present two EPR signals: the first one is located at *ca.* 3381.5 G, corresponding to the EPR $g_1 = 1.932$ signal, while the second one is located at 3421.6 G, corresponding to the EPR $g_2 = 1.910$ signal. Regarding their amplitudes, the EPR g_1 signal presented values of approximately 0.1458, 0.2195 and 0.2435 for SAM2, SAM3, and SAM4, respectively. On the other hand, the EPR g_2 signal values were of *ca.* 0.1870, 0.3057, and 0.1429 for SAM2, SAM3, and SAM4. Note that the behaviour of each center as a function of MAH time is quite different: intensity for g_1 enhances with MAH time, and that of g_2 exhibited a maximum for the

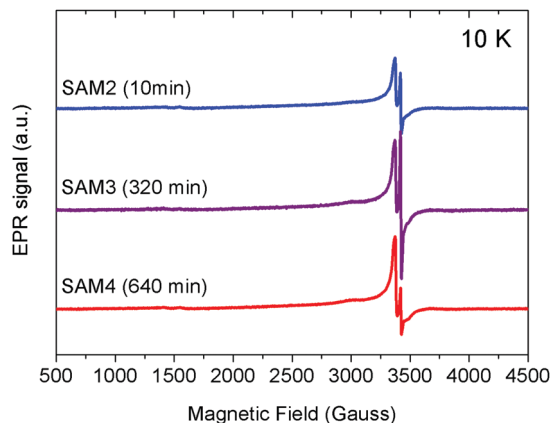


Fig. 7 Electron paramagnetic resonance (EPR) spectra of samples SAM2, SAM3 and SAM4.

SAM3 sample. Based on these findings, it can be attributed that the competition of such centers (relative concentration) led to the reduction in PL emission intensity in the visible region (Fig. 6), and the maximum signal of g_2 can be assigned to the PL emission peak at *ca.* 440 nm for SAM3. In fact, the g_1 signal can be assigned to the peak at approximately 440 nm, and the g_2 to another one at approximately 510 nm. The sum of both emission bands shows a maximum around 470 nm for the SAM2 sample.

4. Conclusions

The main conclusions of the present work can be summarized as follows. (i) The results point out the capability of the MAH method in preparing pristine SrTiO₃ powders in a short time and at a relatively lower temperature. (ii) The combination of thermal and non-thermal effects present during MAH treatment provides ideal conditions for obtaining a pristine SrTiO₃ phase. (iii) The MAH method is not simply used to reduce the reaction time and temperature but also to suppress side reactions, improving the reproducibility. The results obtained by XRD, XANES and XPS techniques confirmed that this treatment is effective in eliminating spurious phases, unlike conventional annealing performed in an electric oven. (iv) FE-SEM images reveal that the crystal growth process along the MAH route occurs *via* an assembly process, forming crystalline SrTiO₃ powders with cube-like morphologies. XPS, EPR and PL results indicated that the increase in the treatment time contributes to a decrease in the defects found in the SrTiO₃ structure with concomitant enhancement of crystallization in the MAH route. (v) Finally, the present results go beyond the specific SrTiO₃ compound and can be extended to many ternary and more complex perovskite based oxides.

Author contributions

All authors have given the approval to the final version of the manuscript.

Conflicts of interest

There are no conflicts to declare.

Acknowledgements

We would like to thank Mr Rorivaldo Camargo for operating the FE-SEM microscope and Prof. Otaciro R. Nascimento (IFSC/USP) for the EPR measurements. This research was partially performed at the Brazilian Laboratory of Synchrotron Radiation (LNLS; Project XAFS-20180311) and the Brazilian Nanotechnology National Laboratory (LNNano; Project XPS-22956), both in Campinas, SP, Brazil. The authors are also grateful for the financial support from the Brazilian research funding institutions CAPES (finance code 88887.197794/2018-00 and 001), CNPq (grant no. 442076/2014-2, 311463/2017-7 and 405140/2018-5), FAPESP and FAPESP (grant no. 2013/07296-2; 2017/12437-5). Prof. Juan Andrés

acknowledges the financial support of the Universitat Jaume I (project UJIB2016-25), the Generalitat Valenciana (project PrometeoII/2014/022, ACOMP/2014/270, and ACOMP/2015/1202), and the Ministerio de Economía y Competitividad, Spain, (Project CTQ2015-65207-P).

Notes and references

- 1 A. S. Bhalla, R. Guo and R. Roy, The perovskite structure – a review of its role in ceramic science and technology, *Mater. Res. Innovations*, 2000, **4**, 3–26.
- 2 S. Komarneni, R. Roy and Q. H. Li, Microwave-hydrothermal synthesis of ceramic powders, *Mater. Res. Bull.*, 1992, **27**, 1393–1405.
- 3 H. Y. Hwang, Perovskites: Oxygen vacancies shine blue, *Nat. Mater.*, 2005, **4**, 803–804.
- 4 H.-J. Kim and J.-H. Lee, Highly sensitive and selective gas sensors using p-type oxide semiconductors: Overview, *Sens. Actuators, B*, 2014, **192**, 607–627.
- 5 G. Zhang, G. Liu, L. Wang and J. T. S. Irvine, Inorganic perovskite photocatalysts for solar energy utilization, *Chem. Soc. Rev.*, 2016, **45**, 5951–5984.
- 6 L. F. da Silva, A. C. Catto, W. Avansi Jr., L. S. Cavalcante, V. R. Mastelaro, J. Andrés, K. Aguir and E. Longo, Acetone gas sensor based on α -Ag₂WO₄ nanorods obtained *via* a microwave-assisted hydrothermal route, *J. Alloys Compd.*, 2016, **683**, 186–190.
- 7 L. F. da Silva, A. C. Catto, W. Avansi Jr, L. S. Cavalcante, J. Andres, K. Aguir, V. R. Mastelaro and E. Longo, A novel ozone gas sensor based on one-dimensional (1D) α -Ag₂WO₄ nanostructures, *Nanoscale*, 2014, **6**, 4058–4062.
- 8 A. C. Catto, L. F. da Silva, M. I. B. Bernardi, S. Bernardini, K. Aguir, E. Longo and V. R. Mastelaro, Local Structure and Surface Properties of Co_xZn_{1-x}O Thin Films for Ozone Gas Sensing, *ACS Appl. Mater. Interfaces*, 2016, **8**, 26066–26072.
- 9 L. F. da Silva, W. Avansi Jr, A. C. Catto, J. E. F. S. Rodrigues, M. I. B. Bernardi and V. R. Mastelaro, The Role of Nb Addition in TiO₂ Nanoparticles: Phase Transition and Photocatalytic Properties, *Phys. Status Solidi A*, 2018, **125**, 1800321.
- 10 D. Segal, *Chemical synthesis of ceramic materials*, 1997, vol. 7, pp. 1297–1305.
- 11 D. M. G. Leite, L. F. da Silva, A. L. J. Pereira and J. H. Dias da Silva, Nanocrystalline Ga_{1-x}Mn_xN films grown by reactive sputtering, *J. Cryst. Growth*, 2006, **294**, 309–314.
- 12 Y.-T. Tseng, J.-C. Lin, Y.-J. Ciou and Y.-R. Hwang, Fabrication of a Novel Microsensor Consisting of Electrodeposited ZnO Nanorod-Coated Crossed Cu Micropillars and the Effects of Nanorod Coating Morphology on the Gas Sensing, *ACS Appl. Mater. Interfaces*, 2014, **6**, 11424–11438.
- 13 M. Baghbanzadeh, L. Carbone, P. D. Cozzoli and C. O. Kappe, Microwave-Assisted Synthesis of Colloidal Inorganic Nanocrystals, *Angew. Chem., Int. Ed.*, 2011, **50**, 11312–11359.
- 14 I. Bilecka and M. Niederberger, Microwave chemistry for inorganic nanomaterials synthesis, *Nanoscale*, 2010, **2**, 1358–1374.

- 15 A. Goktaş, A. Tumbul and F. Aslan, Grain size-induced structural, magnetic and magnetoresistance properties of $\text{Nd}_{0.67}\text{Ca}_{0.33}\text{MnO}_3$ nanocrystalline thin films, *J. Sol-Gel Sci. Technol.*, 2016, **78**, 262–269.
- 16 Y.-H. Huang, Z.-G. Xu, C.-H. Yan, Z.-M. Wang, T. Zhu, C.-S. Liao, S. Gao and G.-X. Xu, Soft chemical synthesis and transport properties of $\text{La}_{0.7}\text{Sr}_{0.3}\text{MnO}_3$ granular perovskites, *Solid State Commun.*, 2000, **114**, 43–47.
- 17 A. Goktas, A. Tumbul and F. Aslan, A new approach to growth of chemically depositable different ZnS nanostructures, *J. Sol-Gel Sci. Technol.*, 2019, **90**, 487–497.
- 18 K. J. Rao, B. Vaidhyanathan and M. Ganguli, and P. a. Ramakrishnan, Synthesis of Inorganic Solids Using Microwaves, *Chem. Mater.*, 1999, **11**, 882–895.
- 19 A. de la Hoz, A. Diaz-Ortiz and A. Moreno, Microwaves in organic synthesis. Thermal and non-thermal microwave effects, *Chem. Soc. Rev.*, 2005, **34**, 164–178.
- 20 W. Shi, S. Song and H. Zhang, Hydrothermal synthetic strategies of inorganic semiconducting nanostructures, *Chem. Soc. Rev.*, 2013, **42**, 5714–5743.
- 21 Y.-J. Zhu and F. Chen, Microwave-Assisted Preparation of Inorganic Nanostructures in Liquid Phase, *Chem. Rev.*, 2014, **114**, 6462–6555.
- 22 A. L. J. Pereira, L. Gracia, A. Beltrán, P. N. Lisboa-Filho, J. H. D. da Silva and J. Andrés, Structural and Electronic Effects of Incorporating Mn in TiO_2 Films Grown by Sputtering: Anatase versus Rutile, *J. Phys. Chem. C*, 2012, **116**, 8753–8762.
- 23 M. L. Moreira, V. M. Longo, W. Avansi, M. M. Ferrer, J. Andrés, V. R. Mastelaro, J. A. Varela and E. Longo, Quantum Mechanics Insight into the Microwave Nucleation of SrTiO_3 Nanospheres, *J. Phys. Chem. C*, 2012, **116**, 24792–24808.
- 24 L. F. da Silva, W. Avansi Jr, J. Andrés, C. Ribeiro, M. L. Moreira, E. Longo and V. R. Mastelaro, Long-range and short-range structures of cube-like shape SrTiO_3 powders: microwave-assisted hydrothermal synthesis and photocatalytic activity, *Phys. Chem. Chem. Phys.*, 2013, **15**, 12386–12393.
- 25 M. L. Moreira, G. P. Mambrini, D. P. Volanti, E. R. Leite, M. O. Orlandi, P. S. Pizani, V. R. Mastelaro, C. O. Paiva-Santos, E. Longo and J. A. Varela, Hydrothermal Microwave: A New Route to Obtain Photoluminescent Crystalline BaTiO_3 Nanoparticles, *Chem. Mater.*, 2008, **20**, 5381–5387.
- 26 J. Sun, W. Wang and Q. Yue, Review on Microwave-Matter Interaction Fundamentals and Efficient Microwave-Associated Heating Strategies, *Materials*, 2016, **9**, 231.
- 27 L. F. da Silva, W. Avansi Jr, M. L. Moreira, A. Mesquita, L. J. Q. Maia, J. Andrés, E. Longo and V. R. Mastelaro, Relationship between Crystal Shape, Photoluminescence, and Local Structure in SrTiO_3 Synthesized by Microwave-Assisted Hydrothermal Method, *J. Nanomater.*, 2012, **2012**, 890397.
- 28 I. Bilecka, L. Luo, I. Djerdj, M. D. Rossell, M. Jagodic, Z. Jaglicic, Y. Masubuchi, S. Kikkawa and M. Niederberger, Microwave-Assisted Nonaqueous Sol-Gel Chemistry for Highly Concentrated ZnO-Based Magnetic Semiconductor Nanocrystals, *J. Phys. Chem. C*, 2011, **115**, 1484–1495.
- 29 G. A. Tompsett, W. C. Conner and K. S. Yngvesson, Microwave Synthesis of Nanoporous Materials, *ChemPhysChem*, 2006, **7**, 296–319.
- 30 M. Godinho, C. Ribeiro, E. Longo and E. R. Leite, Influence of Microwave Heating on the Growth of Gadolinium-Doped Cerium Oxide Nanorods, *Cryst. Growth Des.*, 2008, **8**, 384–386.
- 31 V. M. Longo, A. T. de Figueiredo, S. de Lazaro, M. F. Gurgel, M. G. S. Costa, C. O. Paiva-Santos, J. A. Varela, E. Longo, V. R. Mastelaro, F. S. DE Vicente, A. C. Hernandez and R. W. A. Franco, Structural conditions that leads to photoluminescence emission in SrTiO_3 : An experimental and theoretical approach, *J. Appl. Phys.*, 2008, **104**, 23515.
- 32 J. Li, S. Li, F. Liu, M. A. Alim and G. Chen, The origin of varistor property of SrTiO_3 -based ceramics, *J. Mater. Sci.: Mater. Electron.*, 2003, **14**, 483–486.
- 33 O. K. Tan, W. Cao, Y. Hu and W. Zhu, Nano-structured oxide semiconductor materials for gas-sensing applications, *Ceram. Int.*, 2004, **30**, 1127–1133.
- 34 J. H. Haeni, P. Irvin, W. Chang, R. Uecker, P. Reiche, Y. L. Li, S. Choudhury, W. Tian, M. E. Hawley, B. Craigo, A. K. Tagantsev, X. Q. Pan, S. K. Streiffer, L. Q. Chen, S. W. Kirchoefer, J. Levy and D. G. Schlom, Room-temperature ferroelectricity in strained SrTiO_3 , *Nature*, 2004, **430**, 758–761.
- 35 M. Moniruddin, K. Afroz, Y. Shabdan, B. Bizri and N. Nuraje, Hierarchically 3D assembled strontium titanate nanomaterials for water splitting application, *Appl. Surf. Sci.*, 2017, **419**, 886–892.
- 36 L. F. da Silva, O. F. Lopes, V. R. de Mendonça, K. T. G. Carvalho, E. Longo, C. Ribeiro and V. R. Mastelaro, An Understanding of the Photocatalytic Properties and Pollutant Degradation Mechanism of SrTiO_3 Nanoparticles, *Photochem. Photobiol.*, 2016, **92**, 371–378.
- 37 V. R. Calderone, A. Testino, M. T. Buscaglia, M. Bassoli, C. Bottino, M. Viviani, V. Buscaglia and P. Nanni, Size and Shape Control of SrTiO_3 Particles Grown by Epitaxial Self-Assembly, *Chem. Mater.*, 2006, **18**, 1627–1633.
- 38 L. F. da Silva, L. J. Q. Maia, M. I. B. Bernardi, J. A. Andrés and V. R. Mastelaro, An improved method for preparation of SrTiO_3 nanoparticles, *Mater. Chem. Phys.*, 2011, **125**, 168–173.
- 39 L. F. da Silva, W. Avansi, M. L. Moreira, J. Andres, E. Longo and V. R. Mastelaro, Novel $\text{SrTi}_{1-x}\text{Fe}_x\text{O}_3$ nanocubes synthesized by microwave-assisted hydrothermal method, *CrystEngComm*, 2012, **14**, 4068–4073.
- 40 L. F. da Silva, M. I. B. Bernardi, L. J. Q. Maia, G. J. M. Frigo and V. R. Mastelaro, Synthesis and thermal decomposition of $\text{SrTi}_{1-x}\text{Fe}_x\text{O}_3$ ($0.0 \leq x \leq 0.1$) powders obtained by the polymeric precursor method, *J. Therm. Anal. Calorim.*, 2009, **97**, 173–177.
- 41 L. F. da Silva, V. R. Mastelaro, A. C. Catto, C. A. Escanhoela Jr., S. Bernardini, S. C. Zílio, E. Longo and K. Aguir, Ozone and nitrogen dioxide gas sensor based on a nanostructured $\text{SrTi}_{0.85}\text{Fe}_{0.15}\text{O}_3$ thin film, *J. Alloys Compd.*, 2015, **638**, 374–379.
- 42 L. F. da Silva, J.-C. M'Peko, J. Andrés, A. Beltrán, L. Gracia, M. I. B. Bernardi, A. Mesquita, E. Antonelli, M. L. Moreira and V. R. Mastelaro, Insight into the Effects of Fe Addition

- on the Local Structure and Electronic Properties of SrTiO₃, *J. Phys. Chem. C*, 2014, **118**, 4930–4940.
- 43 M. Bender, E. Gagaoudakis, E. Douloufakis, E. Natsakou, N. Katsarakis, V. Cimalla, G. Kiriakidis, E. Fortunato, P. Nunes, A. Marques and R. Martins, Production and characterization of zinc oxide thin films for room temperature ozone sensing, *Thin Solid Films*, 2002, **418**, 45–50.
- 44 M. L. Moreira, E. C. Paris, G. S. do Nascimento, V. M. Longo, J. R. Sambrano, V. R. Mastelaro, M. I. B. Bernardi, J. Andrés, J. A. Varela and E. Longo, Structural and optical properties of CaTiO₃ perovskite-based materials obtained by microwave-assisted hydrothermal synthesis: An experimental and theoretical insight, *Acta Mater.*, 2009, **57**, 5174–5185.
- 45 A. Michalowicz, J. Moscovici, D. Muller-BouvetDiane and K. Provost, MAX: Multiplatform Applications for XAFS, *J. Phys.: Conf. Ser.*, 2009, **190**, 12034.
- 46 S. Aydogan, M. Erdemoğlu, A. Aras, G. Uçar and A. Özkan, Dissolution kinetics of celestite (SrSO₄) in HCl solution with BaCl₂, *Hydrometallurgy*, 2006, **84**, 239–246.
- 47 A. C. Catto, L. F. da Silva, C. Ribeiro, S. Bernardini, K. Aguir, E. Longo and V. R. Mastelaro, An easy method of preparing ozone gas sensors based on ZnO nanorods, *RSC Adv.*, 2015, **5**, 19528–19533.
- 48 A. M. Ruiz, G. Dezanneau, J. Arbiol, A. Cornet and J. R. Morante, Insights into the Structural and Chemical Modifications of Nb Additive on TiO₂ Nanoparticles, *Chem. Mater.*, 2004, **16**, 862–871.
- 49 R. V. Vedrinskii, V. L. Kraizman, A. A. Novakovich, Ph. V. Demekhin and S. V. Urazhdin, Pre-edge fine structure of the 3d atom K x-ray absorption spectra and quantitative atomic structure determinations for ferroelectric perovskite structure crystals, *J. Phys.: Condens. Matter*, 1998, **10**, 9561.
- 50 D. Barreca, D. Bekermann, E. Comini, A. Devi, R. A. Fischer, A. Gasparotto, C. Maccato, C. Sada, G. Sberveglieri and E. Tondello, Urchin-like ZnO nanorod arrays for gas sensing applications, *CrystEngComm*, 2010, **12**, 3419–3421.
- 51 V. Krayzman, I. Levin, J. C. Woicik, D. Yoder and D. A. Fischer, Effects of local atomic order on the pre-edge structure in the Ti K X-ray absorption spectra of perovskite CaTi_{1-x}Zr_xO₃, *Phys. Rev. B: Condens. Matter Mater. Phys.*, 2006, **74**, 224104.
- 52 M. Ye, M. Wang, D. Zheng, N. Zhang, C. Lin and Z. Lin, Garden-like perovskite superstructures with enhanced photocatalytic activity, *Nanoscale*, 2014, **6**, 3576–3584.
- 53 G. Canu and V. Buscaglia, Hydrothermal synthesis of strontium titanate: thermodynamic considerations, morphology control and crystallisation mechanisms, *CrystEngComm*, 2017, **19**, 3867–3891.
- 54 W. Avansi Jr, L. J. Q. Maia, C. Ribeiro, E. R. Leite and V. R. Mastelaro, Local structure study of vanadium pentoxide 1D-nanostructures, *J. Nanopart. Res.*, 2011, **13**, 4937.
- 55 S. Zhang, D. Guo, M. Wang, M. S. Javed and C. Hu, Magnetism in SrTiO₃ before and after UV irradiation, *Appl. Surf. Sci.*, 2015, **335**, 115–120.
- 56 L. Gu, H. Wei, Z. Peng and H. Wu, Defects enhanced photocatalytic performances in SrTiO₃ using laser-melting treatment, *J. Mater. Res.*, 2017, **32**, 748–756.
- 57 O. Lobacheva, Y. M. Yiu, N. Chen, T. K. Sham and L. V. Goncharova, Changes in local surface structure and Sr depletion in Fe-implanted SrTiO₃ (001), *Appl. Surf. Sci.*, 2017, **393**, 74–81.
- 58 R. P. Vasquez, SrTiO₃ by XPS, *Surf. Sci. Spectra*, 1992, **1**, 129–135.
- 59 V. V. Atuchin, V. G. Kesler, N. V. Pervukhina and Z. Zhang, Ti 2p and O 1s core levels and chemical bonding in titanium-bearing oxides, *J. Electron Spectrosc. Relat. Phenom.*, 2006, **152**, 18–24.
- 60 H. Tan, Z. Zhao, W. Zhu, E. N. Coker, B. Li, M. Zheng, W. Yu, H. Fan and Z. Sun, Oxygen Vacancy Enhanced Photocatalytic Activity of Perovskite SrTiO₃, *ACS Appl. Mater. Interfaces*, 2014, **6**, 19184–19190.
- 61 J.-C. Dupin, D. Gonbeau, P. Vinatier and A. Levasseur, Systematic XPS studies of metal oxides, hydroxides and peroxides, *Phys. Chem. Chem. Phys.*, 2000, **2**, 1319–1324.
- 62 A. E. Souza, G. T. A. Santos, B. C. Barra, W. D. Macedo, S. R. Teixeira, C. M. Santos, A. M. O. R. Senos, L. Amaral and E. Longo, Photoluminescence of SrTiO₃: Influence of Particle Size and Morphology, *Cryst. Growth Des.*, 2012, **12**, 5671–5679.
- 63 W. F. Zhang, Z. Yin, M. S. Zhang, Z. L. Du and W. C. Chen, Roles of defects and grain sizes in photoluminescence of nanocrystalline SrTiO₃, *J. Phys.: Condens. Matter*, 1999, **11**, 5655.
- 64 A. Rubano, D. Paparo, F. M. Granozio, U. Scotti di Uccio and L. Marrucci, Blue luminescence of SrTiO₃ under intense optical excitation, *J. Appl. Phys.*, 2009, **106**, 103515.
- 65 G. Blasse, On the luminescence of SrTiO₃ and related titanates, *Mater. Res. Bull.*, 1983, **18**, 525–528.
- 66 H. Trabelsi, M. Bejar, M. P. F. Graça, M. A. Valente, M. J. Soares and N. A. Sobolevi, Raman, EPR and ethanol sensing properties of oxygen-vacancies SrTiO_{3-δ} compounds, *Appl. Surf. Sci.*, 2017, **426**, 386–390.